Author ORCID: https://orcid.org/0009-0009-6367-4655

Corresponding author: O. L. Konovalov <konovalovol@bsu.by>

Date: August 17, 2026

Explicit Structural Modeling of Geological Horizons Near Fault Networks

O. L. Konovalov

Abstract

This article extends the approach of [1] — constructing a geological horizon surface near a single tectonic fault — to the case of a system of arbitrary, including intersecting, faults. The generalization requires solving four subtasks: formalization of the fault system as a simplicial complex, construction of the modeling domain as a γ-neighborhood of the cut graph on the triangulation, replacement of retriangulation by mesh deformation, and generalization of the free boundary movement formula to three cases of sub-edge endpoint type combinations. Thanks to the edge-based discretization of the area functional [1], the problem reduces to independent systems of linear algebraic equations at each iteration — one for each subdomain. Results of testing on real geological objects are presented.
Keywords: structural model, horizon surface, fault system, simplicial complex, topological cut, free boundary, edge-based discretization, mesh deformation, modeling domain.

1 Introduction

In the preceding work [1], a mathematically grounded approach to constructing a geological horizon surface in the vicinity of a single tectonic fault was proposed. The problem of reconstructing the modeled part of the surface was reduced to a mixed boundary value problem with a free boundary (BVPFB) in a variational formulation. An original edge-based discretization of the area functional was developed, yielding a linear problem for any value of the parameter $\theta \in [0, 1]$, which controls the balance between smoothness and realism of the surface. A practical approach to handling self-intersection of cut edges was described, naturally extending the algorithm to the case of reverse faults (thrusts).

However, real geological objects are rarely characterized by single faults. As a rule, faults form systems with complex topological structure: faults may intersect, forming junctions of various configurations. Applying the approach [1] to each fault independently does not ensure structural consistency in intersection zones. An algorithm treating the fault system as a single topological object is required.

Existing approaches to structural modeling in the vicinity of faults can be divided into two groups. Implicit methods (implicit surface modeling) define the horizon surface as a level set of a scalar field constructed by interpolation from data [5, 6, 7, 8]. They are robust but poorly controllable: the intersection of the surface with a fault is determined a posteriori, which may lead to geometric contradictions [9, 10]. Moreover, implicit methods operate with three-dimensional scalar fields, which requires constructing a three-dimensional triangulation of the entire modeling domain. Accurate accounting of

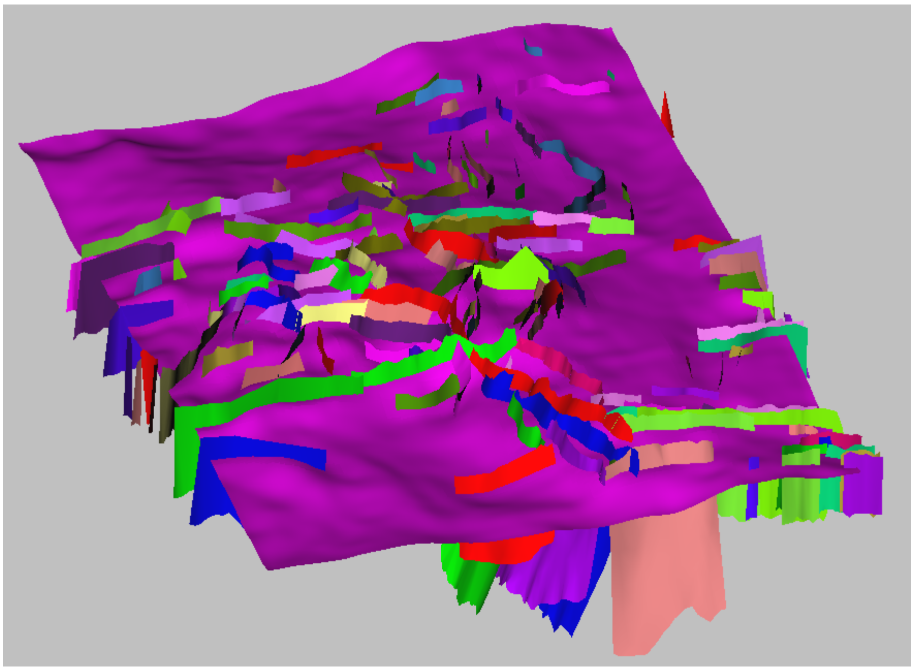

Figure 1: Fault network of a real field: intersecting faults form a complex topological structure.

discontinuities along faults within the implicit approach also requires preliminary processing (cleaning) of fault surfaces to ensure correct intersections. Explicit methods (explicit surface modeling) construct the surface directly as a triangulation. These include methods based on DSI (Discrete Smooth Interpolation) [11, 12, 14] and GRP (Gradual Deformation) [13]. Explicit methods provide direct control of topology; however, cutting along faults within these methods is generally performed heuristically, without reduction to a mathematically correct boundary value problem [15]. Despite these limitations, the explicit approach is of significant interest due to direct control of surface geometry and topology; in our opinion, this direction is underrated. The present work continues the line of explicit methods within the variational formulation proposed in [1].

2 Problem Statement

In [1], the problem of constructing a horizon surface in the vicinity of a single normal fault was reduced to a mixed boundary value problem with a free boundary [16, 17] in a variational formulation [18]. The sought surface is a minimizer of a weighted combination of the Dirichlet energy and the area functional ($\theta \in [0, 1]$), with boundary conditions on Γ_0 (matching with the reliable part of the horizon) and on free boundaries Γ_i (coincidence with the fault surface: $u = w_i$). The edge-based discretization reduces the problem to a system of linear algebraic equations (SLAE) $A\mathbf{u} = \mathbf{b}$; the matrix A is assembled from the topological adjacency of simplices and does not depend on the geometric embedding of the triangulation. The iterative algorithm: solve the SLAE, move free boundaries (project onto the fault), retriangulate, check termination criteria. Numerical experiments [1] demonstrated the algorithm's applicability to thrust faults as well, using a special retriangulation mechanism.

Note that in [1] the domain Ω is assumed to be given. In practice, such a domain is not present in the input data: there is a horizon surface constructed from seismic data and fault surfaces. The modeling domain — the part of the horizon surface to be reconstructed in the vicinity of faults — is constructed in the present article on the triangulation (Sect. 4).

The present work generalizes the approach [1] to a system of arbitrary faults, including intersecting ones. The discrete problem preserves its structure; the generalization requires solving four subtasks.

Formalization of the fault system. The fault system must be described as a single topological object — a simplicial complex admitting the construction of a cut graph and a topological cut of the triangulation. It is required to define the conditions that the system satisfies and to describe the topology of the domain with cuts. Solved in Sect. 3.

Construction of the modeling domain and topological cut. It is required to construct a triangulation containing the cut graph as constraints, define the modeling domain through the parameter γ, and perform the topological cut. Solved in Sect. 4.

Modification of retriangulation. In [1], upon self-intersection of cut edges (thrust), the domain Ω was split into two subdomains, each retriangulated independently. With a system of intersecting faults, the number of intersection points and, consequently, the number of subdomains can be significant, making this approach practically inapplicable. A mechanism preserving the cut topology without domain splitting is required. Solved in Sect. 5 (mesh deformation).

Modification of free boundary movement. With a fault system, cut edges are split into sub-edges by intersection vertices. The movement of sub-edge endpoints depends on their type: an endpoint on the fault boundary ($\mathrm{ind}(v) = 1$) or at an intersection vertex ($\mathrm{ind}(v) > 2$); the definition of the topological index $\mathrm{ind}(v)$ is given in Sect. 4. It is required to generalize the consistent boundary transformation formula [1] to all combinations of endpoint types. Solved in Sect. 6.

3 Formalization of the Fault System

3.1 Requirements for structural surfaces

The concepts of combinatorial topology [2] are used; the necessary definitions are recalled below. A *simplicial complex* K is a finite set of simplices in $\mathbb{R}^m$ such that together with each simplex it contains all of its faces, and any two simplices intersect along a common face (possibly empty). The union of all simplices of the complex K is called the *polyhedron* $|K|$. A homogeneous n-dimensional polyhedron is called *strongly connected* if any two of its n-simplices can be joined by an n-chain — a sequence of n-simplices in which consecutive elements share a common $(n-1)$-face. The orthogonal projection onto the xy-plane is denoted by $\pi_{xy} : \mathbb{R}^3 \to \mathbb{R}^2$.

Consider the requirements for the surfaces entering the structural model: the horizon surface and the fault surfaces. Compared to [1], these requirements are extended.

Functional requirements

1. *Non-parametric (functional) representation.* The horizon surface and the fault surfaces have representations as functions $u : \Omega \to \mathbb{R}$ and $w_i : \Omega_{w_i} \to \mathbb{R}$, where $\Omega, \Omega_{w_i} \subset \mathbb{R}^2$ are bounded closed sets, and the graphs of these functions project bijectively onto the xy-plane. The boundary $\partial\Omega_{w_i}$ may partially coincide with $\partial\Omega$

or extend beyond it: a fault may extend beyond the edge of the horizon domain. This requirement was introduced in [1] for a single fault; here it is extended to all surfaces of the system.

2. *Z-monotonicity.* The fault surfaces w_i have no stationary points ($\nabla w_i = 0$) in the interior of the domain Ω_{w_i}. This is a necessary condition for the correctness of the procedure of projecting free boundary points onto the fault surface [1]: at a stationary point, the denominator $\nabla w_i \cdot \mathbf{n}$ in the projection formula vanishes. In practice, violation of Z-monotonicity (appearance of stationary points on the fault surface) requires correction of the fault surface at the cleaning stage — for example, a local change of dip.

Each fault in the system is described in two representations. The *polyhedral representation* — fault i is given by a two-dimensional strongly connected polyhedron W_i in $\mathbb{R}^3$ with simplicial complex K_{W_i}. This representation is used for computing intersections of faults with each other and with the horizon surface, i.e., for constructing the topological structure of cuts. The *functional representation* (requirement 1) — fault i is described by the function w_i. This representation is used for formulating boundary conditions and for the procedure of projecting free boundary points onto the fault surface in the variational problem. Thus, the polyhedral representation serves the topological part of the algorithm, while the functional one serves the variational part.

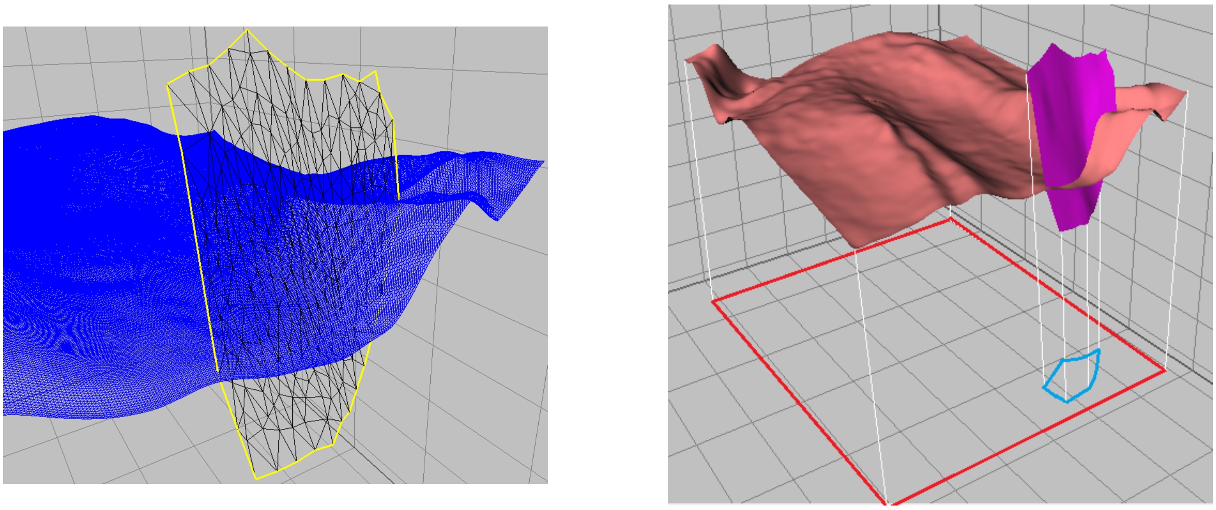

Figure 2: Two representations of geometry: (a) polyhedral; (b) functional.

The transition from the polyhedral representation to the functional one proceeds as follows. The projection π_{xy} of the vertices and edges of the polyhedron W_i onto the xy-plane yields a two-dimensional triangulation $\mathcal{T}_h(\Omega_{w_i})$ of the domain Ω_{w_i}; the z-coordinates of the polyhedron's vertices become the values of the piecewise-linear function w_i at the nodes of this triangulation. When requirement 1 (bijectivity of the projection) is satisfied, this transition is correct and reversible: W_i is recovered as the graph of the function w_i in $\mathbb{R}^3$. Thus, the variational problem (Sect. 2) can be formulated in finite-dimensional form: the unknowns are the values of u at the nodes of the triangulation, and the system matrix is assembled by the edge-based discretization of internal edges [1].

Fictitious fault

In addition to active faults satisfying the functional requirements, a *fictitious fault* is included in the simplicial complex — a vertical cylinder W_{fict} constructed on the outer boundary Γ_0 of the modeling domain, with vertical boundaries Z^-, Z^+, encompassing the depths of the faults and the horizon. The fictitious fault satisfies the topological conditions of consistency and transversality (Sect. 3.2), but has no functional representation and does not participate in the variational problem. Its role is to provide intersection edges $W_i \cap W_{\text{fict}}$ that serve as guides for the movement of cut-edge endpoints reaching Γ_0 (Sect. 6).

3.2 Fault system as a geometric complex

Individual faults satisfying the requirements of Sect. 3.1 form a *fault system* if the following conditions are met.

Consistency conditions

The union of the simplicial complexes of active faults $K_{W_1} \cup \ldots \cup K_{W_N}$ and the fictitious fault $K_{W_{\text{fict}}}$ is a simplicial complex [2] (simplices from different complexes intersect along a common face or do not intersect). The pairwise intersection $W_i \cap W_j$ ($i \neq j$, including W_{fict}) is a strongly connected one-dimensional polyhedron (a connected polyline).

The pairwise intersection condition excludes fault tangency (zero-dimensional intersection): in practice, such configurations require preliminary separation of faults at the cleaning stage.

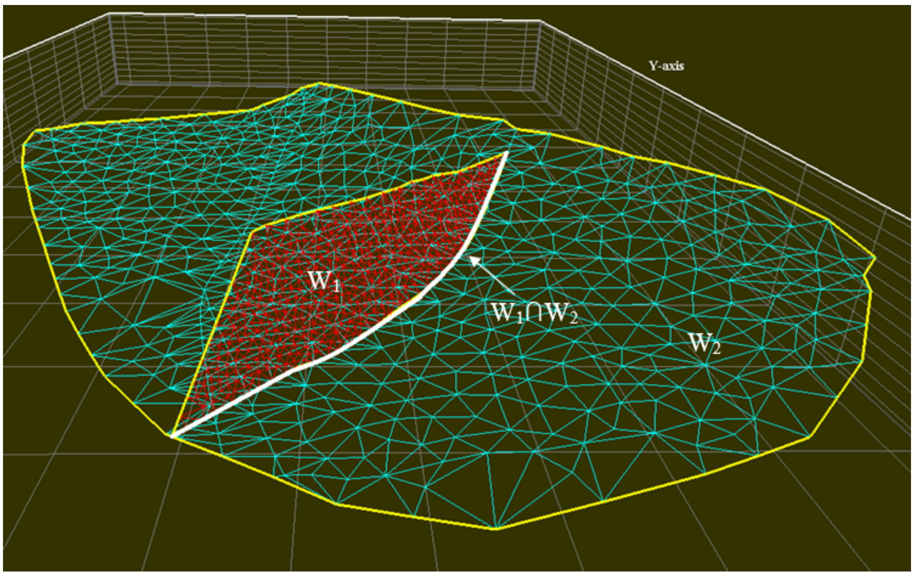

Figure 3: Correct intersection of two faults: the white polyline — part of the boundary ∂W_1 of the first fault — is present in the triangulation of the second fault W_2 as triangulation edges. The intersection $W_1 \cap W_2$ is a strongly connected one-dimensional polyhedron.

Transversality conditions

Let $u_0 : \Omega \to \mathbb{R}$ be the solution of the variational problem without cuts [1]. The function u_0 on the triangulation of the domain Ω defines a two-dimensional polyhedron $U \subset \mathbb{R}^3$ —

the horizon surface. The mutual arrangement of U and the fault polyhedra must satisfy the conditions:

3. the intersection $U \cap W_i$ for each active i is a one-dimensional polyhedron (polyline) whose endpoints belong to ∂W_i, $W_i \cap W_j$ ($j \neq i$, including W_{fict}), or ∂U;

4. the intersection $U \cap W_i \cap W_j$ for any $i \neq j$ is a zero-dimensional polyhedron (possibly empty).

Conditions 3–4 are checked after constructing U.

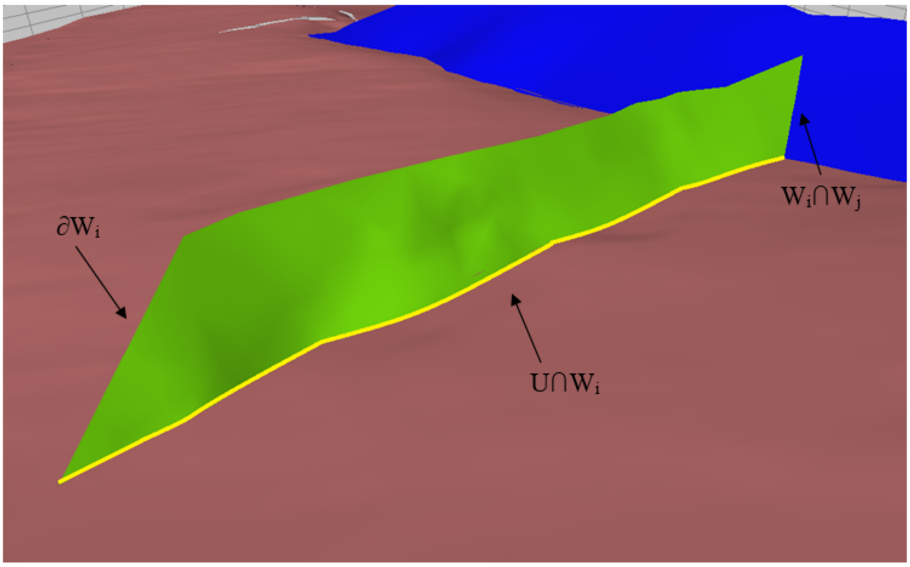

Figure 4: Transversality condition: the intersection $U \cap W_i$ is a one-dimensional polyhedron (polyline). The endpoints of the polyline belong to ∂W_i (fault tip), $W_i \cap W_j$ (fault intersection).

3.3 Cut polyhedron and cut graph

Define the *cut polyhedron* as the intersection of the horizon polyhedron U with the union of *active* fault polyhedra:

$$G = U \cap (W_1 \cup \cdots \cup W_N). \tag{1}$$

The fictitious fault is not included in the cut polyhedron.

Lemma 1. Under requirement 1 and conditions 1–4 (Sect. 3.2), the projection $g = \pi_{xy}(G)$ is a planar graph; the endpoints of the graph edges belong to $\partial\Omega_{w_i}$ or Γ_0.

Proof. Represent G as $G = (U \cap W_1) \cup \cdots \cup (U \cap W_N)$. By condition 3, each $U \cap W_i$ is a one-dimensional polyhedron. By condition 4, the intersection $(U \cap W_i) \cap (U \cap W_j) = U \cap W_i \cap W_j$ for $i \neq j$ is a zero-dimensional polyhedron. The union of one-dimensional polyhedra whose pairwise intersections are zero-dimensional is a one-dimensional polyhedron.

By requirement 1, the projection π_{xy} is bijective on U (each point $(x, y) \in \Omega$ corresponds to a unique point $(x, y, u_0(x, y)) \in U$). Thus $\pi_{xy}|_U : U \to \Omega$ is a homeomorphism. Since $G \subset U$, the restriction $\pi_{xy}|_G : G \to g$ is a bijection. The projection π_{xy} is linear, so each simplex K_G maps to a simplex K_g of the same dimension — a simplicial isomorphism $K_G \cong K_g$ is established.

Planarity. By requirement 1, $\pi_{xy}|_U$ is injective. Two edges of G that do not share a point in $\mathbb{R}^3$ cannot project to intersecting segments on xy: the intersection point (x_0, y_0) in the plane corresponds to a unique point $(x_0, y_0, u_0(x_0, y_0))$ in G, and if both edges pass through it, they share a point in $\mathbb{R}^3$ — a contradiction. Thus, the projection creates no new intersections; the only meeting points of edges of g are the projections of the zero-dimensional sets $U \cap W_i \cap W_j$ (condition 4), which are vertices of the graph. Edges of g intersect only at vertices — g is a planar graph without self-intersections.

The endpoints of the graph edges belong to $\partial\Omega_{w_i}$ or Γ_0 (condition 3: the endpoints of $U \cap W_i$ belong to ∂W_i, $W_i \cap W_j$ $(j \neq i)$, or ∂U; the projection of ∂W_i gives $\partial\Omega_{w_i}$, the projection of ∂U gives Γ_0). $\square$

Corollary. The simplicial isomorphism $K_G \cong K_g$, established in the proof, means that the structure of the cut graph g in the xy-plane uniquely corresponds to the structure of the cut polyhedron G in $\mathbb{R}^3$. This allows performing all topological constructions (triangulation cut, domain partition) in the two-dimensional plane without recourse to three-dimensional geometry.

The projection $g = \pi_{xy}(G)$ is called the *cut graph*.

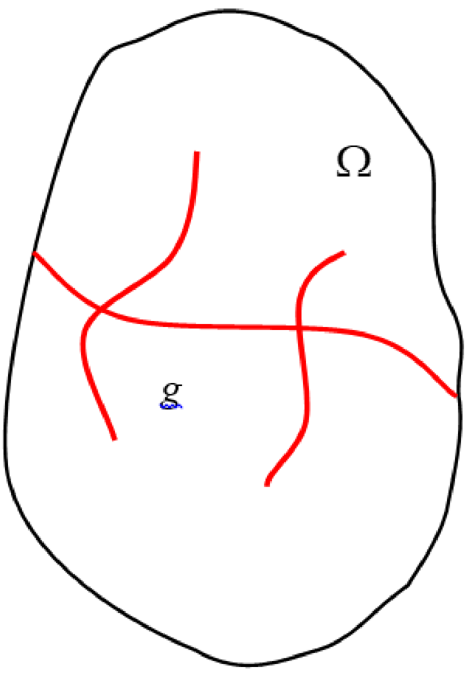

Figure 5: Cut graph for three intersecting faults. The graph divides Ω into two domains.

Let Γ_0 be the outer boundary of the domain Ω [1]. Edges of the cut graph g may reach Γ_0 (where a fault exits to the domain boundary) or terminate on $\partial\Omega_{w_i}$ (where a fault ends inside Ω). Edges reaching Γ_0 divide the domain Ω into connected regions, each of which has access to Γ_0. Edges not reaching Γ_0 form internal boundaries (holes) in the corresponding regions.

If the graph g contains independent cycles, each cycle delineates a separate region bounded only by cut edges; such a region has no access to Γ_0. In this case, other methods for specifying boundary conditions would be required, which would significantly complicate the general formulation of the boundary value problem. Therefore, it is further assumed that the graph g contains no cycles. This assumption can be justified, among other things, by the fact that for typical fault configurations, cut edges on a single horizon rarely form closed contours.

The formulated functional requirements (Sect. 3.1), the consistency and transversality conditions (Sect. 3.2), and the assumption of absence of cycles in the cut graph constitute a complete set of conditions that the structural surfaces must satisfy. Ensuring this set at the preprocessing stage of raw seismic data — *cleaning* — includes ensuring correct intersections of fault surfaces, verifying horizon transversality with the fault system, checking for the absence of cycles in the cut graph, and, if necessary, correcting fault surfaces and modifying the boundary of the domain Ω.

4 Initial Triangulation and Topological Cut

The horizon polyhedron U and the fault polyhedra W_i are obtained from seismic data. The cut graph $G = U \cap (W_1 \cup \cdots \cup W_N)$ (formula (1)) and its projection $g = \pi_{xy}(G)$ are constructed directly from the original surfaces.

A *constrained Delaunay triangulation* [3] T_0 of the horizon domain is constructed, containing the vertices and edges of the graph g as constraints: the vertices of the graph are vertices of the triangulation, the edges of the graph are edges of the triangulation.

The modeling domain is defined by the parameter γ: triangles of T_0 whose centroid is at a distance no greater than γ from the graph g contain unknowns (the values of u are determined by solving the SLAE); vertices at a distance greater than γ from g are fixed with values from the original seismic surface (Dirichlet condition). The set of fixed vertices forms the outer boundary Γ_0. The parameter γ is set by the geologist and determines the width of the reconstruction zone along the faults. The fictitious fault (Sect. 3.1) is constructed on Γ_0.

4.1 Topological cut

The *topological cut* of the triangulation T_0 along the edges of the graph g is a procedure generalizing the algorithm from [1] to the case of multiple intersecting cuts.

The number of cut edges incident to a vertex v of the graph g is called the *topological index* $\mathrm{ind}(v)$. For cut endpoints $\mathrm{ind}(v) = 1$; for interior points of an edge $\mathrm{ind}(v) = 2$; for fault intersection vertices $\mathrm{ind}(v) > 2$. At an intersection vertex v, $\mathrm{ind}(v)$ copies are created — one for each incident subdomain. Each triangle of T_0 is assigned a subdomain; the graph vertices in the triangle are replaced by the corresponding copies.

Lemma 2. Let T_0 be a triangulation of a connected domain containing the planar graph g as a subcomplex. Then Algorithm 1 partitions T_0 into strongly connected components: for each resulting triangulation T_j^0, any two triangles are connected by a chain of triangles in which consecutive elements share a common edge in T_j^0.

Proof. Consider the dual graph $D(T_0)$: vertices are triangles of T_0, edges connect triangles sharing a common edge. Since T_0 triangulates a connected domain, $D(T_0)$ is connected.

Let $D_g \subset D(T_0)$ be the dual edges corresponding to edges of the graph g. Removing D_g from $D(T_0)$ partitions it into connected components $C_1, \ldots, C_M$. By construction, each C_j is strongly connected.

We prove that the component labels in Algorithm 1 (steps 1–3) give exactly $C_1, \ldots, C_M$.

($\Rightarrow$) If $t_1, t_2 \in C_j$, there exists a path in $D(T_0) \setminus D_g$: a chain $t_1 = s_0, \ldots, s_n = t_2$, in which consecutive triangles share edges not belonging to g. The centroids of $s_0, \ldots, s_n$

Algorithm 1 Topological cut of a triangulation along the cut graph

Require: Triangulation T_0; cut graph g (subset of edges of T_0)
Ensure: Set of triangulations $\{T_j^0\}_{j=1}^M$ — strongly connected components

Build the dual graph $D(T_0)$: vertices — triangles, edges — pairs of triangles sharing an edge
Remove from $D(T_0)$ the edges corresponding to edges of g
Find connected components; label each triangle t with the number j of its component
for each vertex $v \in V(g)$ **do**
    Among the triangles incident to v, collect the set J_v of distinct labels j
    $\mathrm{ind}(v) \leftarrow |J_v|$
    Create $\mathrm{ind}(v)$ copies of vertex v: $v^{(j)}$, $j \in J_v$
for each triangle $t \in T_0$ with label j **do**
    for each vertex v_i of triangle t **do**
        if $v_i \in V(g)$ **then**
            Replace v_i with copy $v_i^{(j)}$
return $\{T_j^0\}_{j=1}^M$

form a continuous path in $\mathbb{R}^2$ not crossing g; hence, t_1 and t_2 receive the same label.

($\Leftarrow$) If t_1, t_2 lie in the same face F of the planar subdivision by the graph g, their centroids are interior points of F. Since F is an open connected set, there exists a path in F from $\mathrm{cent}(t_1)$ to $\mathrm{cent}(t_2)$ avoiding all vertices of T_0. This path crosses only edges of T_0 not belonging to g; the sequence of crossed triangles yields a chain in $D(T_0) \setminus D_g$ connecting t_1 and t_2.

Thus the component labels give exactly $C_1, \dots, C_M$, and each component is strongly connected. □

Strong connectivity is necessary for assembling the SLAE: the edge-based discretization [1] forms the matrix from the adjacency of simplices through edges; under weak connectivity (connection only through a vertex), the matrix blocks become disconnected and the SLAE degenerates. The constrained Delaunay triangulation guarantees that the cut graph edges are edges of T_0, ensuring the applicability of the lemma.

After the algorithm is executed, we obtain a set of triangulations $\{T_j^0\}_{j=1}^M$ — one for each subdomain. The topology is fixed and does not change further. For each subdomain, the iterative algorithm (Sect. 5–7) operates independently.

As a result of the topological cut, the cut edges are split into *sub-edges* — segments between consecutive vertices of the graph g. A sub-edge is bounded by two vertices: a cut endpoint ($\mathrm{ind}(v) = 1$), an interior point ($\mathrm{ind}(v) = 2$), or an intersection vertex ($\mathrm{ind}(v) > 2$). The sub-edge structure is used in the free boundary movement (Sect. 6).

5 Modification of Retriangulation

The topological cut (Sect. 4) partitions the triangulation T_0 into subdomains $\{T_j^0\}$; each subdomain has its own free boundary Γ_j (cut edges) and a fixed boundary Γ_0 (vertices at distance $> \gamma$ from g). Below, the deformation step is described, performed for each subdomain independently.

In [1], retriangulation is performed at each iteration after moving the free boundary. With a system of intersecting faults, retriangulation may change the cut topology — the number of subdomains, the topological indices of vertices. Since the cut topology is fixed at the topological cut stage (Sect. 4) and must not change, retriangulation is inapplicable.

Instead, *mesh deformation* is applied: the displacement of free boundaries is propagated to interior nodes by solving a Laplace problem for the displacement field. The triangulation topology (simplex adjacency) remains unchanged; only the node coordinates change.

The displacements dx, dy for all nodes of each subdomain are computed by solving two Laplace problems:

$$\Delta(dx) = 0, \qquad \Delta(dy) = 0 \qquad \text{in the subdomain,} \tag{2}$$

$$dx = dy = 0 \qquad \text{on } \Gamma_0\text{, except at cut-edge endpoints,} \tag{3}$$

$$dx = \Delta x_i,\ dy = \Delta y_i \qquad \text{on } \Gamma_i, \tag{4}$$

where $(\Delta x_i, \Delta y_i)$ are the known displacements of the free boundary points Γ_i, computed at the boundary movement step. Here Γ_0 refers to the vertices at distance $> \gamma$ from g, fixed with values from the seismic surface. At the vertices of Γ_0 corresponding to cut-edge endpoints reaching Γ_0, a tangential displacement along Γ_0 is specified (along the intersection edge $W_i \cap W_{\text{fict}}$ with the fictitious fault, Sect. 6); the remaining vertices of Γ_0 are fixed. After solving, all nodes are shifted: $P_m \to P_m + (dx_m, dy_m)$.

For the discretization of (2), the same edge-based discretization of the Dirichlet energy [1] is used as for the main problem. The system matrix for (dx, dy) has the same structure as the matrix A (same topology, same edges); only the right-hand sides differ. This allows performing a single LU factorization and applying it to different right-hand sides — for u and for (dx, dy).

The algorithm by construction does not allow topology changes: deformation occurs within existing subdomains, and free boundary points are projected onto fault surfaces without the possibility of forming new intersections. If the real geometry requires a change of the cut topology, the algorithm stops according to one of the termination criteria (Sect. 7).

For large displacements, individual triangles may degenerate — lose orientation (negative area). In this case, *local remeshing* is applied: edge flips and node insertion/deletion in degenerated regions, with cut edges preserved as constraints. In new nodes, the displacement field values are interpolated from the previous step. The updated triangulation becomes the initial one for the next iteration; the matrix A is recomputed.

6 Modification of Free Boundary Movement

In [1], free boundary movement was described for two types of points: interior ($\text{ind}(v) = 2$, movement along the normal with projection onto the fault) and boundary ($\text{ind}(v) = 1$, movement along $\partial\Omega_w$). With a fault system, cut edges are split into sub-edges by intersection vertices, which requires generalization.

Each cut edge $\gamma_{i,s}$ ($s = 1, 2$; $i = 1, \dots, N$) is a *chain of sub-edges*:

$$\gamma_{i,s} = \gamma_{i,s}^{(1)} \cup \gamma_{i,s}^{(2)} \cup \dots \cup \gamma_{i,s}^{(p_{i,s})} \tag{5}$$

separated by *intersection vertices* — points at which fault i intersects other faults on the horizon surface. Sub-edges correspond to edges of the cut graph g (corollary of Lemma 1).

The number of cut edges incident to a vertex v is called the *topological index* $\mathrm{ind}(v)$ (Sect. 4). For cut endpoints $\mathrm{ind}(v) = 1$; for interior points of an edge $\mathrm{ind}(v) = 2$; for intersection vertices $\mathrm{ind}(v) > 2$.

At an intersection vertex v ($\mathrm{ind}(v) = k > 2$), the cut edges of $k/2$ faults meet. Since v is a common vertex of the triangulations of all intersecting faults (a consequence of condition 1, Sect. 3.2), the fault surface values are consistent at it: $w_{i_1}(v) = \cdots = w_{i_{k/2}}(v)$, where $i_1, \ldots, i_{k/2}$ are the intersecting faults.

The movement of a sub-edge depends on the types of its endpoints. Three cases are possible.

Case 1: both endpoints $\mathrm{ind}(v) = 1$. As in [1]: interior points ($\mathrm{ind}(v) = 2$) move along the normal to the cut curve with projection onto the fault surface w_i; endpoints ($\mathrm{ind}(v) = 1$) move along a guide determined by Table 1, until the condition $u = w_i$ is satisfied.

Case 2: one endpoint $\mathrm{ind}(v) = 1$, *the other* $\mathrm{ind}(v) = k > 2$. The endpoint with $\mathrm{ind}(v) = 1$ moves along a guide (Table 1). The endpoint with $\mathrm{ind}(v) > 2$ moves *along the intersection edge* of the faults, which is explicitly present in the triangulations as a common 1-simplex.

Case 3: both endpoints $\mathrm{ind}(v) > 2$. Both endpoints move along the corresponding intersection edges (possibly of different fault pairs).

In all three cases, the structure of the consistent boundary transformation formula is the same as in [1]:

$$\mathbf{v}(t) = (1 - \alpha_1(t) - \alpha_2(t))\,\mathbf{n}(t) + \alpha_1(t)\,\mathbf{b}_1 + \alpha_2(t)\,\mathbf{b}_2, \tag{6}$$

with weight functions $\alpha_1(t) = (1-t)^2$, $\alpha_2(t) = t^2$. The choice of quadratic weight functions is inherited from [1], where it is shown to ensure smooth coupling of the movement at the sub-edge endpoints. Only the *source* of the projective vectors $\mathbf{b}_1, \mathbf{b}_2$ changes depending on the type and location of the endpoints (Table 1).

Table 1: Projective vectors: types and sources.

Projective vector type	Source
$\mathrm{ind}(v) = 1$, $\partial\Omega_{w_i}$	Projection along $\partial\Omega_{w_i}$ until $u = w_i$ [1]
$\mathrm{ind}(v) = 1$, Γ_0	Movement along $W_i \cap W_{\text{fict}}$ (tangential to Γ_0) until $u = w_i$
$\mathrm{ind}(v) > 2$	Movement along the fault intersection edge (common 1-simplex)

The endpoints on Γ_0 are mobile thanks to the fictitious fault: the intersection edge $W_i \cap W_{\text{fict}}$ — the trace of fault i on the cylinder — is explicitly present in the simplicial complex as a common 1-simplex and serves as a guide for tangential movement along Γ_0.

7 Summary Algorithm

At each iteration $k = 0, 1, 2, \ldots$, for each subdomain:

1. *Solve the SLAE.* The matrix A^k and the right-hand side $\mathbf{b}^k$ are assembled for the current triangulation (the topology is the same as at the topological cut; only the node coordinates change). The SLAE $A^k\mathbf{u}^k = \mathbf{b}^k$ is solved — yielding the values

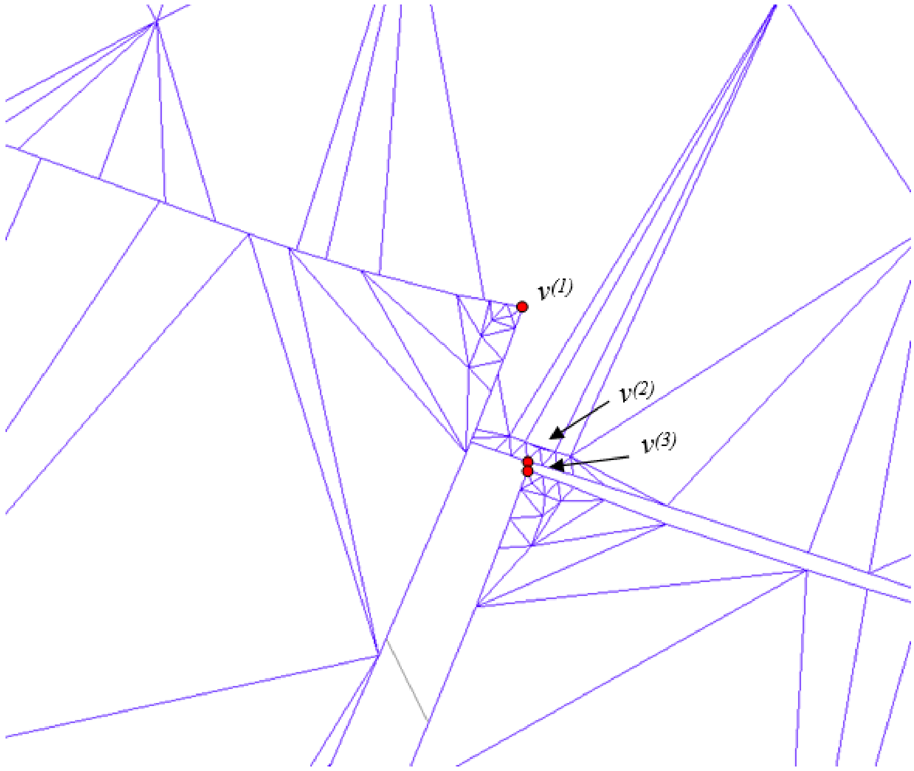

Figure 6: Movement of a fault intersection vertex. Each copy $v^{(j)}$ moves in its own subdomain subject to constraints from the corresponding faults.

of u^k at the unknown nodes (distance $\leq \gamma$ from g). The nodes of Γ_0 (distance $> \gamma$) are fixed with values from the seismic surface. A direct sparse LU factorization is used (SuperLU [4]).

2. *Move free boundaries* (Sect. 6).

3. *Mesh deformation* (Sect. 5): solve the SLAE for (dx, dy) (same matrix, different right-hand side), shift nodes.

4. *Recompute parameters* t_e, s_e of the edge-based discretization [1] from the new node coordinates. The sparsity pattern of the matrix A does not change; only the numerical values of the coefficients change.

5. *Local remeshing* upon triangle degeneration (Sect. 5).

At the first iteration ($k = 0$), the initial values of u^0 at the nodes are taken from the original seismic surface.

Termination criteria. The algorithm provides four types of termination. The first is normal convergence; the remaining three are diagnostic signals for the geologist, indicating the need to correct the input data. The conditions are checked in the order given.

Type 0: convergence (normal termination). The maximum vertical deviation on the free boundaries drops below a prescribed threshold ε_{tol}:

$$\varepsilon^k = \max_{\substack{i=1,\dots,N \\ p\in\Gamma_i^k}} \left|u^k(p) - u^{k-1}(p)\right| < \varepsilon_{\text{tol}}. \tag{7}$$

The free boundary has reached a stable position on the fault surface with the required accuracy. The algorithm terminated successfully.

Type 1: stagnation (boundary oscillation). The deviation stops decreasing without reaching the threshold:

$$\varepsilon^k \geq \varepsilon^{k-1}, \qquad \varepsilon^k \geq \varepsilon_{\text{tol}}. \tag{8}$$

The free boundary oscillates between positions without converging to a fixed one. This signals a geometric contradiction requiring correction of the model parameters.

Type 2: projection failure. When moving a free boundary point, the projection formula onto the fault surface yields no solution: the point exits the domain Ω_{w_i}, or the denominator $\nabla w_i \cdot \mathbf{n}$ vanishes (violation of Z-monotonicity, requirement 2). This signals an insufficient dip angle of the fault surface.

Type 3: intersection vertex reached. When moving a sub-edge endpoint along the intersection edge of two faults, the point reaches the end of the intersection edge and cannot be projected further. This signals an incorrect fault junction geometry in the intersection zone.

Algorithm 2 Constructing a horizon surface in the vicinity of a fault system

Require: Fault polyhedra $W_1, \ldots, W_N$; seismic surface; parameters θ, γ, ε_{tol}
Ensure: Horizon surface consistent with all faults

Construct the cut graph:
  $G \leftarrow U \cap (W_1 \cup \cdots \cup W_N)$ ▷ from input data
  $g \leftarrow \pi_{xy}(G)$
Initial triangulation:
  Build constrained Delaunay T_0 with g as constraints ▷ Sect. 4
  Label vertices of T_0: distance $\leq \gamma$ from g — unknowns; $> \gamma$ — Dirichlet (Γ_0)
  Topological cut (Algorithm 1) $\to \{T_j^0\}$ ▷ Sect. 4
For each subdomain (independently):
  $u^0 \leftarrow$ seismic surface values
  Iterations ($k = 0, 1, 2, \ldots$):
    Solve SLAE $A^k \mathbf{u}^k = \mathbf{b}^k$ ▷ surface
    Move free boundaries ▷ Sect. 6
    Solve SLAE for (dx, dy); shift nodes ▷ Sect. 5
    Recompute t_e, s_e; [remesh if degenerate]
    Check termination criteria ▷ type 0–3
Result: u^k on the unified grid

Computational details. The algorithm is implemented in C++ using the libraries **SuperLU 5.2.1** (sparse LU factorization), **Triangle 1.6** (constrained Delaunay triangulation) [3], and **Eigen 3.4** (vector and matrix operations). Tests were performed on an Intel Xeon E5-2680 v4 workstation (2.4 GHz, 14 cores, 64 GB RAM). The average time per iteration ranged from ≈0.8 s (Model 1) to ≈4.2 s (Model 3). Parameters: $\theta = 0.5$, γ — twice the grid cell diagonal, $\varepsilon_{\text{tol}} = 0.1$ m.

8 Testing and Validation

The algorithm was tested on several structural models of real large fields. The models were selected based on the criterion of maximum representativeness: they differ significantly from each other and maximally cover the range of real geological situations.

Variable parameters: number of faults, number of intersections, grid step. The parameter θ is fixed (sensitivity to θ was investigated in [1]); $\varepsilon_{\mathrm{tol}} = 0.1$ m. The parameter γ is set individually for each fault in the range from 3 to 5 grid steps.

Table 2: Characteristics of real geological models.

Model	Step, m	Faults	Intersect.	Min. angle	Avg. angle
Fang	200.0	4	0	33.0	44.0
Bohai	150.0	7	2	35.0	41.0
KrSloboda	200.0	15	6	22.0	37.4
Ashtart	100.0	27	8	27.1	35.7
Chicontepec	150.0	11	4	30.0	42.0
Chesapeak	120.0	45	0	25.0	39.0
OGX	200.0	5	1	38.0	46.0

Table 3: Testing results: average and maximum number of iterations (over subdomains), average displacement of free boundary points, average vertical deviation, number of remeshings, termination type.

Model	Avg. iter.	Max. iter.	$\bar{d}$ (m)	$\bar{\varepsilon}$ (m)	Remesh.	Termination
Fang	10	15	0.06	0.07	0	Type 0 (conv.)
Bohai	12	19	0.05	0.06	2	Type 0 (conv.)
KrSloboda	16	22	0.07	0.08	5	Type 2 (proj.)
Ashtart	13	18	0.05	0.07	3	Type 2 (proj.)
Chicontepec	14	20	0.06	0.07	4	Type 0 (conv.)
Chesapeak	15	21	0.06	0.08	4	Type 3 (vert.)
OGX	9	14	0.04	0.05	0	Type 0 (conv.)

Analysis of the results on real geological models shows:

1. Normal convergence (type 0) was achieved in models 1, 2, 5, and 7 — with 9–14 iterations and average deviation $\bar{\varepsilon} \leq 0.07$ m. Termination by diagnostic criteria (types 1–3) occurred in models 3, 4, and 6; in each case, the termination type corresponds to the geological characteristics of the model (small dip angle — type 2; complex intersection — type 3).

2. The algorithm operates robustly in the presence of intersecting faults (models 2–6 with 1–6 intersections). The number of iterations grows with the number of intersections but remains within 9–22.

3. Mesh deformation (instead of retriangulation) ensured robustness in all tests. Local remeshing was required only in models 2–6 (2–5 cases over all iterations, all successfully handled). In models 1 and 7 (without intersections or with a single intersection), remeshing was not required.

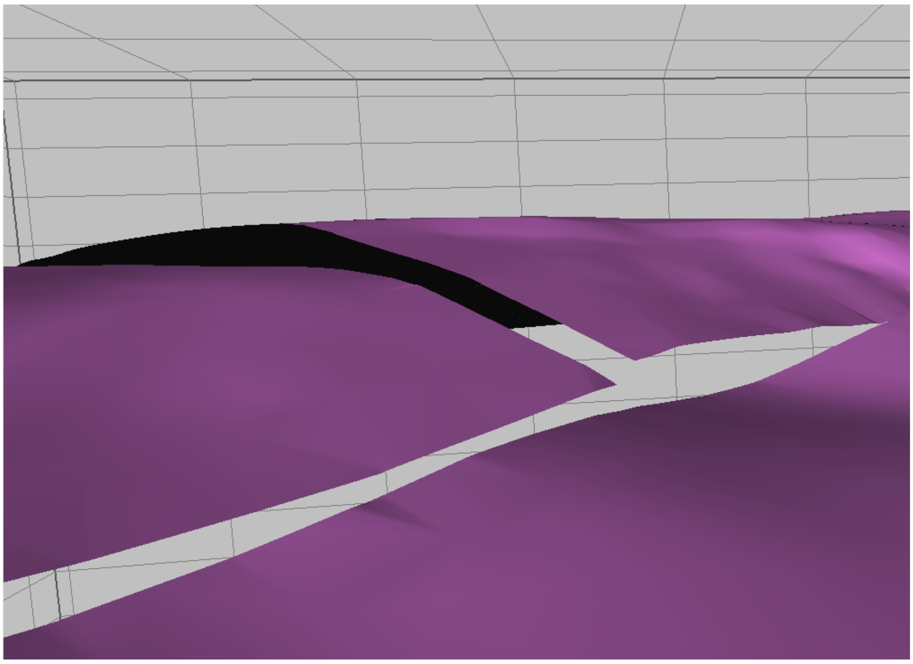

Figure 7: Algorithm result for a T-shaped fault intersection shown in Fig. 3: the horizon surface is reconstructed in the vicinity of both faults, free boundaries are consistent with fault surfaces.

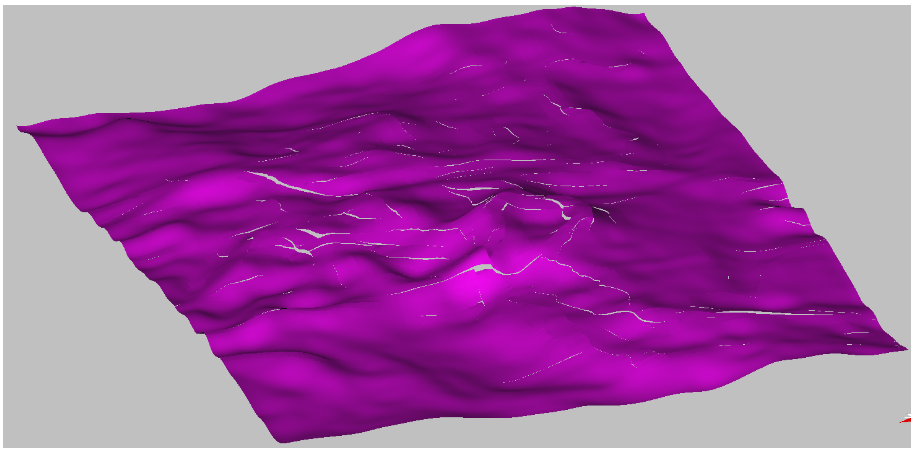

Figure 8: Resulting horizon surfaces obtained by the algorithm for the fault system shown in Fig. 1.

4. The algorithm is sensitive to the minimum dip angle of fault surfaces. Faults with small angles ($< 30°$) lead to an increase in the number of iterations and termination by type 2 (projection failure). This is related to the deterioration of the accuracy of the free boundary point projection procedure onto the fault surface at small angles.

5. Thrust faults with small dip angles have significant horizontal extent and, within structural modeling, are generally considered as additional horizon surfaces; nevertheless, processing such faults within the proposed approach is possible provided sufficient dip angle after cleaning.

9 Discussion

Limitations.

1. *Small dip angles* ($< 30°$). At small dip angles of fault surfaces, the accuracy of the projection procedure of free boundary points onto the fault surface deteriorates, and the node displacement during deformation increases, which may lead to termination by type 2 (projection failure).

2. *Interactive nature of the algorithm.* The algorithm provides four types of termination (Sect. 7): normal convergence (type 0) and three diagnostic types (1–3). The diagnostic types are not failures — each indicates to the geologist a specific direction for correcting the input data (Table 4). After correction, the algorithm is restarted. Such an interactive mode is natural for structural modeling: the algorithm does not replace geological judgment but points to problematic zones.

3. *Absence of cycles in the cut graph.* The assumption of absence of cycles (Sect. 3) excludes configurations in which cut edges form closed contours. For such configurations, other methods for specifying boundary conditions would be required.

4. *Consistency condition at intersection vertices.* The equality of fault surface values at intersection vertices is a consequence of the simplicial complex. If exact equality is not achieved after cleaning (for example, due to interpolation errors), additional correction of fault surfaces is required at the preprocessing stage.

5. *Branching faults.* The case where one fault terminates on the surface of another (T-shaped intersection, $\mathrm{ind}(v) = 3$) is formally covered by the proposed formalization. However, practical testing of this case requires separate consideration.

Table 4: Diagnostic interpretation of algorithm termination types.

Type	Diagnostic meaning	Recommended action
0 (conv.)	—	Result is ready
1 (stagn.)	Geometric contradiction	Change θ, extend γ
2 (proj.)	Insufficient fault dip	Extend fault, modify w_i
3 (vert.)	Incorrect intersection geometry	Correct intersection, extend Ω

Comparison with implicit methods. The proposed approach has two key differences. First, unlike implicit methods, in which the intersection of the horizon surface with a fault is determined a posteriori (with the risk of geometric contradictions), in the proposed formulation the cut is specified as part of the boundary value problem — a free boundary whose position is determined together with the surface. This ensures topological correctness by construction. Second, the proposed approach operates with a two-dimensional problem, whereas implicit methods require constructing a three-dimensional scalar field. This reduces computational cost and simplifies control of surface geometry.

Parallelization. Since the subdomains are independent, the SLAEs for different subdomains can be solved in parallel. At each iteration, for each subdomain, two systems are solved (for u and for (dx, dy)), using the same LU factorization. The natural level of parallelism is one subdomain per compute node.

10 Conclusion

An algorithm for constructing a horizon surface in the vicinity of a system of arbitrary faults, including intersecting ones, has been proposed — a generalization of the approach [1] for a single fault. The generalization required solving four subtasks.

Formalization of the fault system (Sect. 3). The fault system is described as a simplicial complex; consistency and transversality conditions are defined, and the cut graph is constructed as a planar graph (Lemma 1). The key property of the simplicial complex — the explicit presence of intersection edges in the triangulations of all intersecting faults as common simplices — ensures exact construction of the cut graph and geometric consistency at intersection vertices without numerical solution of consistency equations. The fictitious fault (a vertical cylinder on Γ_0) is included in the simplicial complex but not in the cut polyhedron; it provides intersection edges $W_i \cap W_{\text{fict}}$ that serve as guides for the movement of cut-edge endpoints reaching Γ_0.

Initial triangulation and topological cut (Sect. 4). A constrained Delaunay triangulation T_0 containing the cut graph g as constraints is constructed from seismic data. The modeling domain is defined by the parameter γ: vertices close to g are unknowns, far ones are Dirichlet. The topological cut (Algorithm 1) partitions T_0 into strongly connected subdomains (Lemma 2), for each of which a SLAE is independently assembled and solved.

Mesh deformation (Sect. 5). The retriangulation used in [1] is replaced by mesh deformation — node displacement at fixed topology. This is dictated by feasibility: retriangulation with a system of intersecting faults leads to uncontrolled changes in the cut topology. The price is the inability to change the cut structure during iterations.

Free boundary movement (Sect. 6). The consistent boundary transformation formula [1] is generalized to three cases of sub-edge endpoint type combinations ($\text{ind}(v) = 1$ or $\text{ind}(v) > 2$). The endpoints on Γ_0 are mobile thanks to the fictitious fault: they move along the edges $W_i \cap W_{\text{fict}}$ (tangential to Γ_0).

Termination criteria (Sect. 7). The algorithm distinguishes normal convergence (type 0 — the deviation drops below ε_{tol}) and three diagnostic termination types — stagnation, projection failure, intersection vertex reached — each of which indicates to the geologist a specific direction for correcting the input data.

Thanks to the edge-based discretization [1], the problem at each iteration reduces to independent SLAEs — one for each subdomain. The SLAE matrix is assembled from the topological adjacency of simplices and does not depend on the geometric embedding, which allows working in the two-dimensional plane and obtaining the result (a three-dimensional triangulation) by lifting to $\mathbb{R}^3$.

The testing results on real models of large fields (6–15 faults, 0–6 intersections) confirm the practical applicability of the algorithm. The algorithm operates robustly when the minimum dip angle of fault surfaces exceeds 30°; at smaller angles, special processing is required.

Further generalization to the case of cycles in the cut graph (thrusts, closed cut contours) will require other methods for specifying boundary conditions and the development of the theory of cellular CW-complexes for describing the topology of cuts of arbitrary complexity.

References

[1] O. L. Konovalov, "Model and algorithm for constructing a horizon surface in the vicinity of a single fault," EarthArXiv, 2026. doi:10.31223/X58Z1X.

[2] E. I. Yakovlev, *Introduction to Combinatorial Topology* (in Russian), Nizhny Novgorod: Nizhny Novgorod Univ. Press, 2004.

[3] J. R. Shewchuk, "Triangle: Engineering a 2D quality mesh generator and Delaunay triangulator," in *Applied Computational Geometry: Towards Geometric Engineering*, LNCS 1148, 1996, pp. 203–222.

[4] J. W. Demmel, S. C. Eisenstat, J. R. Gilbert, X. S. Li, J. W. H. Liu, "A supernodal approach to sparse partial pivoting," SIAM J. Matrix Anal. Appl., vol. 20, no. 3, 1999, pp. 720–755.

[5] C. Lajaunie, G. Courrioux, L. Manuel, "Foliation fields and 3D cartography in geology: principles of a method based on potential field interpolation," Math. Geol., vol. 29, no. 4, 1997, pp. 571–604.

[6] P. Calcagno, J. P. Chilès, G. Courrioux, A. Guillen, "Geological modelling from field data and prior knowledge," Phys. Earth Planet. Inter., vol. 171, no. 1–4, 2008, pp. 158–169.

[7] M. Irakarama, G. Laurent, J. Renaudeau, G. Caumon, "Finite difference implicit modeling of geological structures," Math. Geosci., vol. 53, 2020, pp. 785–808.

[8] J. Renaudeau, E. Malvesin, F. Maerten, G. Caumon, "Implicit structural modeling by minimization of the bending energy with moving least squares functions," Math. Geosci., vol. 51, 2019, pp. 693–724.

[9] G. Caumon, P. Collon-Drouaillet, C. Le Carlier de Veslud, J. Sausse, "Surface-based 3D modeling of geological structures," Math. Geosci., vol. 41, no. 8, 2009, pp. 927–945.

[10] G. Laurent, G. Caumon, A. Bouziat, "A parametric method to model 3D faults and fault networks," Math. Geosci., vol. 45, 2013, pp. 759–775.

[11] J.-L. Mallet, "Discrete smooth interpolation," ACM Trans. Graph., vol. 8, no. 2, 1989, pp. 121–144.

[12] J.-L. Mallet, *Geomodeling*, Oxford: Oxford Univ. Press, 2002.

[13] L. G. Hu, “Gradual deformation and Kalman filter,” Math. Geosci., vol. 41, 2009, pp. 311–326.

[14] T. Frank, A.-L. Tertois, J.-L. Mallet, “3D-reconstruction of complex geological interfaces from non-regularly spaced data,” Comput. Geosci., vol. 33, no. 7, 2007, pp. 932–943.

[15] K. B. Sprague, E. A. de Kemp, “Implication of approximating stratigraphic surfaces: a case study from western Canada,” Geosphere, vol. 2, no. 6, 2006, pp. 340–352.

[16] V. N. Monakhov, *Boundary-Value Problems with Free Boundaries for Elliptic Systems of Equations* (in Russian), Novosibirsk: Nauka, 1977.

[17] J. Crank, *Free and Moving Boundary Problems*, Oxford: Clarendon Press, 1987.

[18] R. Courant, *Dirichlet’s Principle, Conformal Mapping, and Minimal Surfaces*, New York: Interscience, 1950.